



Antifouling digital microfluidics using lubricant infused porous film

Journal:	<i>Lab on a Chip</i>
Manuscript ID	LC-ART-03-2019-000289.R2
Article Type:	Paper
Date Submitted by the Author:	28-May-2019
Complete List of Authors:	Geng, Hongyao; University of Pittsburgh, Department of Mechanical Engineering and Materials Science Cho, Sung Kwon; University of Pittsburgh, Mechanical Engineering

ARTICLE

Antifouling digital microfluidics using lubricant infused porous film†

Hongyao Geng and Sung Kwon Cho*

Received 00th January 20xx,
Accepted 00th January 20xx

DOI: 10.1039/x0xx00000x

Electrowetting-driven digital (droplet-based) microfluidics has tremendous impact on lab-on-a-chip applications. However, the biofouling problem impedes the real applications of such digital microfluidics. Here we report an antifouling digital microfluidics by introducing a lubricant infused porous film to electrowetting (more exactly, electrowetting on dielectric or EWOD). Such film minimizes direct contact between droplets and solid surface but provides liquid-liquid contact between droplets and lubricant liquid, which thus prevents unspecific adsorption of biomolecules to the solid surface. We demonstrate the compatibility of the lubricant infused film with EWOD to transport bio droplets. This configuration shows robust and high performance even for long cyclic operations without fouling in a wide range of concentrations of protein solutions. In addition, a variety of conductive droplets, including deionized (DI) water, saline, protein solution, DNA solution, sheep blood, milk, ionic liquid and honey, are examined, similarly showing high performance in cyclic transportations. In addition, using the same electrode patterns used in EWOD, transportations of dielectric (non-conductive) droplets including light crude oil, propylene carbonate and alcohol are also achieved. Such capability of droplet handling without fouling will certainly benefit the practical applications of digital microfluidics in droplet handling, sampling, reaction, diagnosis in clinic medicine, biotechnology and chemistry fields.

Introduction

Digital microfluidics takes individual droplets as the carriers, containers and reaction chambers of many reagents and samples¹⁻⁸. Those droplets can be manipulated by electrowetting on dielectric (EWOD): droplets are created, transported, split, and merged by controlling an array of electrodes⁹⁻¹³. Recently, dielectrowetting is also applied to dielectric as well as conductive fluids to achieve these functions on a single plate¹⁴. These operations endow digital microfluidics with full fluidic functions when compared with its counterpart, conventional channel-based microfluidics, which can dispense, pump, control the volume and mix fluids¹⁵. This method has many unique advantages. First, it can be programmed to control droplets, making it highly flexible and reconfigurable. Second, no mechanical moving components are essentially required including pumps, tubes, valves and connectors, simplifying the structures and peripherals and avoiding the burdensome operations. Third, while the channel-based microfluidics is generally sealed, digital microfluidics allows for direct access to working droplets since it can be operated in an open environment, facilitating many analyzing methods and

applications¹⁶, for example, direct printing of biomolecule on the chip¹⁷.

However, as of today, the application degree of digital microfluidics is not high yet. One of the main problems is biofouling^{11,18}. Cross-contaminations can occur easily during transporting since biomolecules, more prominently with proteins, are prone to adsorb onto the surface¹¹. Thus, the contaminated surface hampers EWOD from actuating droplets. In EWOD-based digital microfluidics, the solid surfaces are generally coated with a hydrophobic layer to reduce the contact angle hysteresis, to have a large span of contact angle change, and thus to facilitate the droplet transporting¹⁹⁻²¹. However, due to the hydrophobic interaction^{22,23}, protein molecules have a higher tendency to adhere to the hydrophobic surface²⁴, eventually rendering a large contact angle hysteresis. Furthermore, the electric field in EWOD accelerates biofouling⁶.

Currently, the EWOD digital microfluidic devices may be classified into two types depending on the filler fluid: oil-filled and air-filled. The oil-filled (commonly silicone oil) devices seem to less suffer from biofouling than the air-filled devices because a thin oil layer temporarily formed between the droplet and the solid hydrophobic surface minimizes physical contact between biomolecules in the droplet and the hydrophobic surface¹⁰. However, such oil-filled devices generally complicate the structure and packaging to completely fill the device with oil and maintain it without any leak. In addition, the oil filler makes devices less compatible with applications which require an air environment.

In the meantime, for the air-filled EWOD, adding additives to droplets relieves biofouling in digital microfluidics to some

Department of Mechanical Engineering and Materials Science, University of Pittsburgh, PA 15261, USA

*skcho@pitt.edu.

† Electronic Supplementary Information (ESI) available. See DOI: 10.1039/x0xx00000x

extent²⁵⁻²⁷, but it may not be favorable in many cases because of introducing additional supplements or contaminations to working fluids. In addition, applying a thin oil film to cloak the droplet surface can reduce the biofouling, but requires more operations^{28,29}. Other methods including tuning pH and electrode polarity³⁰ or synthesizing new coating³¹ also improve the antifouling performance, but the destination of completely and robustly preventing fouling is not reached yet.

To solve the above fouling issues thoroughly, an antifouling surface is required to integrate with digital microfluidics. Such surface should be robust enough to withstand various bio-solutions including proteins, even at high concentrations. Moreover, it should be compatible with EWOD principle in a reasonable range of activating voltages. Inspired by nature, a slippery liquid infused porous surface (SLIPS) was recently reported to repel various liquids, which can also be applied to self-cleaning and anti-fouling³²⁻⁴⁴. The nano-pores in the SLIPS structure effectively hold the infused lubricant oil and minimize its loss. A variety of liquids placed on the top surface, where a thin lubricant liquid film is formed, are free to move laterally⁴⁵⁻⁴⁷. In this case, liquid droplets are separated from the solid surface but in direct contact with the lubrication liquid layer on the SLIPS^{48,49}. The liquid-liquid interaction results in low contact angle hysteresis due to the liquid nature of indefinite shearing^{40,50,51}. Recently, EWOD has been integrated with the SLIPS to decrease contact angle hysteresis⁵²⁻⁵⁴. A low voltage EWOD on the SLIPS was also realized by modifying the surface with perfluorinated silane⁵⁵. However, EWOD with SLIPS has not been evaluated for antibiofouling yet, to the authors' best knowledge.

Here, the air-filler EWOD digital microfluidics is integrated with the SLIPS. Some of the preliminary results were presented in the conference³⁵. The major focus in this article experimentally proves this integration for antifouling with a variety of liquid solutions including DI water, saline solution, ionic liquid, DNA solution, protein solution, whole milk, sheep blood, honey, crude oil, propylene carbonate, and isopropyl alcohol. The anti-biofouling performance of EWOD on the SLIPS is verified for the sessile droplets as well as transporting droplets, both of which are in the air environment. In this configuration, cloaking the droplet surface with the lubricant oil does not occur or is negligible, later evidenced by the spreading power relation and evaporation behaviors. As a result, the present system provides many advantages: easy packaging due to air filler, minimized or no contaminations and no additives to the working droplets. This integration with antibiofouling would be highly beneficial to many fluidic operations of bio droplets, in particular, to the applications requiring droplets in the air environment.

Fabrication and Experimental Method

Device fabrication

As shown in Fig. 1a, an array of hexagonal electrodes is fabricated on the glass substrate for droplet transportation. Note that each hexagonal electrode is split into two sections with a gap in the middle to drive droplets in the co-planar EWOD electrode configuration⁵⁶. Each section of the electrodes can be electrically addressed. Two types of liquid droplets can be actuated by using these electrodes, either conductive or dielectric. The working principle is EWOD for conductive liquids and is liquid dielectrophoresis (L-DEP) for dielectric liquids. As a result, this electrode platform is versatile for real applications, dealing with a wide range of liquids to be manipulated. For the contact angle measurements with sessile droplets, however, a single electrode covering the entire substrate surface is used. The additional layer construction on the electrodes is shown in Fig. 1b. A 2- μm SU-8 layer is coated on top of the electrodes as the dielectric layer to separate lubricant from the electrodes as well as to enhance the electrowetting effect. Note that the dielectric constant (3.2) of SU-8 is larger than that (less than 2) of lubricant. Finally, the SLIPS film is attached to the SU-8 surface to prevent biofouling. The thickness of the film should be small (4.2 μm) to reduce the required electrical voltage. Detailed fabrication process is described below (Supplementary Fig. 1a).

Metal layers (10 nm Cr and 100 nm Au) are deposited by electron-beam evaporation on a cleaned glass wafer. The electrode pattern is made by conventional photolithography, followed by wet etching, using Au etchant and Cr etchant (Sigma Aldrich) in sequence. After that, a 2- μm SU-8 (SU-8 2002, MicroChem) layer is spin-coated at 3000 rpm, heated at 95°C and exposed to ultraviolet light to strengthen the layer.

Next, two options are applied to the SU-8 surface, as shown in Supplementary Figs. 1a and b. The first option (Supplementary Fig. 1a) is that a thin Teflon layer is dip-coated onto the SU-8 surface, which is prepared for the conventional EWOD sample. Before coating, Teflon AF solution (DuPont) is diluted with perfluoro-compound FC-75 solvent (Acros Organics) to achieve a 1 % weight concentration. The second option (Supplementary Fig. 1b) is adding a SLIPS to the SU-8 surface. A piece of porous PTFE film (pore size: 200-500 nm, Zeus) is attached to a thin PDMS slab (2 mm thick), followed by pressing them to the SU-8 surface. To minimize any folds or wrinkles and improve the uniform adhesion between the PTFE and SU-8 layers, a droplet of IPA is placed on the SU-8 surface first, which infuses the porous film by capillarity. After that, the PDMS slab is peeled off, leaving the PTFE film on the device. Then, the infused PTFE film quickly dries at room temperature.

Finally, the SLIPS is formed by dropping a Krytox-103 oil (DuPont, immiscible to aqueous and hydrocarbon liquids) drop to the porous PTFE surface, and removing the excess liquid by gravity for several hours (the samples are vertically aligned). The SLIPS film is more transparent (Supplementary Fig. 1c) after the lubricant is infused.

Regarding the materials used, saline (phosphate buffered), DNA (Isolated from a single female donor placenta and dissolved in water at 1 mg/mL), propylene carbonate, isopropyl alcohol (IPA) and protein powder (fluorescent bovine serum albumin or BSA) were purchased from Sigma-Aldrich. Different

concentrations of BSA proteins (0.02, 1 and 50 mg/mL) were made by dissolving the protein powder into DI water. A digital compact bench scale (ADAM) was used to weigh the powders. Light crude oil was from ONTA, Inc. Ionic liquid (Butyltrimethylammonium 1, 1, 2, 2-tetrafluoroethanesulfonate, 99%) was obtained from IOLITEC, Inc. Whole milk and honey were from local food market. Sheep blood was from University of Pittsburgh.

Experimental setup

In the experiment, a 1 kHz sinusoidal signal is used. A function generator (33220A, Agilent) generates such signal, which is amplified by an amplifier (PZD 700, Trek). The voltage is measured by an oscilloscope (199C, Fluke). In this paper, the measured voltage is denoted by root-mean-square (V_{rms}). The real-time video images are taken using a camera (EO-5310C, Edmund) and a microscope. The contact angle in the images is measured using the Contact Angle plug-in of ImageJ software. The amplified signals to the electrodes are switched on and off by a customized circuit with a microprocessor (MEGA 2560, Arduino), which is connected to a personal computer. The time for voltage application ranges from less than 1 sec to several sec depending on the fluid type.

Results and discussion

Contact angle and contact angle hysteresis

The initial contact angles of conductive droplets on the SLIPS surface are in a suitable range ($> 90^\circ$) for EWOD: 113° for DI water, 115° for BSA solution (1 mg/ml), 110° for DNA solution, 105° for sheep blood, 96° for whole milk, and 114° for honey. The contact angles of dielectric droplets on the SLIPS are 60° for IPA, 88° for propylene carbonate, and 65° for light crude oil.

The contact angle hysteresis is a dynamic parameter to measure the adhesion between a droplet and its contacting surface. When a droplet is moving on a surface, the contact angle on the advancing side (called advancing contact angle) is larger than the equilibrium contact angle. On the other hand, the contact angle on the receding side (called receding contact angle) is smaller than the equilibrium contact angle. The contact angle hysteresis is the difference between the advancing and receding angles, which is commonly referred to as a measure of adhesion and resistance against lateral movements. In particular, when a droplet is transported, the hysteresis is frequently regarded more important than the equilibrium contact angle.

When biofouling occurs on a surface, the surface has very large contact angle hysteresis. As a result, a droplet to be transported is stuck on the surface. As shown in Fig. 2, the contact angle hysteresis of protein droplet (1 mg/mL BSA) is examined on a Teflon surface (Fig. 2a) and SLIPS (Fig. 2b) by adding and withdrawing the fluid using a syringe. On the Teflon surface, the hysteresis is measured to be 92.8° ($= 121.5^\circ - 28.7^\circ$), while on the SLIPS it is 14.4° ($= 116.6^\circ - 102.2^\circ$). These

results indicate that the SLIPS would significantly reduce biofouling. Also note that the tilting angle of 1.5 μL protein droplet is about 20° .

Note that the excessive lubricant oil in the SLIPS was removed by gravity (aligning the device vertically for several hours). This results in the high roughness of the present SLIPS ($\sim 5 \mu\text{m}$) and then the relatively high contact angle hysteresis. Otherwise, the contact angle hysteresis may be close to 0° , as reported⁴⁰. In this case, however, it would be difficult to hold a droplet on a desired spot while the droplet is not actuated. Similarly, a high contact angle hysteresis was reported on the stretched SLIPS⁵⁷. The theoretical apparent contact angle^{58,59} of water droplet on a very thin lubricant oil film can be calculated by the modified Young's equation⁶⁰ $\cos \theta = (\gamma_{OV} - \gamma_{OL}) / \gamma_{eff} = 123.3^\circ$, where $\gamma_{eff} = \gamma_{LV}$ when the spreading power $S_{OL} < 0$, where γ_{LV} , γ_{LO} and γ_{OV} are the interfacial tensions of liquid-air, liquid-oil and oil-air, respectively. The measured static contact angle is 113° . The difference may be attributed to the roughness of the present SLIPS.

Contact angles during droplet evaporation

The effect of contact angle hysteresis is further manifested in the droplet evaporation process, which indirectly evaluates the biofouling as well. The protein droplet (1 mg/ml) evaporation on the SLIPS is compared with that on other solid surfaces: dry porous polytetrafluoroethylene (PTFE) which is superhydrophobic due to surface roughness, and hydrophobic Teflon which is widely used in conventional EWOD digital microfluidics (Fig. 3). As shown in Fig. 3a (Supplementary Video 1), the dried patterns after complete evaporation are different depending on the underneath layers: a "coffee-ring" shape (ring bump at the edge of the pattern) on the dry porous superhydrophobic PTFE surface, a relatively uniform thickness yet large circular pattern on the Teflon film, or a small dot on the SLIPS.

Figures 3b and 3c show how the contact angle changes in each case during evaporation. On the porous PTFE surface, most of the proteins deposit near the edge of the droplet due possibly to Marangoni flow³⁵. The contact angle decreases from 140° to 81.6° . The proteins contaminate the surface easily. Even washing the surface with water was not able to eliminate the adsorbed proteins completely. On the Teflon surface, the finally dried footprint shrinks more than that of the PTFE case, which means the adhesion between the proteins and Teflon surface is weaker than that on the PTFE surface. However, irreversible biofouling still exists. The contact angle of the protein droplet on the Teflon surface changes from 115.6° to 67.2° . As for on the SLIPS, the droplet volume during evaporation is decreasing with time but the measured contact angle stays nearly constant between 113° and 120° . The three-phase contact line can move freely even by small forces generated during evaporation, showing good anti-biofouling performance. Fig. 3d shows the contacting area of the droplet on the SLIPS decreases linearly with time, in agreement with the prediction of the contact angle mode evaporation⁶⁰.

The above evaporation behavior is similar for extremely highly concentrated protein solutions (50 mg/mL). The contact

area of 50 mg/mL protein droplet on the Teflon surface remains almost constant while that on the SLIPS decreases as the droplet is evaporated (Supplementary Video 2 and Supplementary Fig. 2).

Whether or not the lubricant oil cloaks the droplet surface can be determined by the spreading power $S_{OL} = \gamma_{LV} - \gamma_{LO} - \gamma_{OV}$, where γ_{LV} , γ_{LO} and γ_{OV} are the interfacial tensions of liquid-air, liquid-oil and oil-air, respectively. If water ($\gamma_{LV} = 72.4$ mN/m) and lubricant oil (Krytox 103, $\gamma_{OV} = 17.4$ mN/m, $\gamma_{LO} = 57.2$ mN/m) are used, $S_{OL} = 72.4 - 57.2 - 17.4 = -2.2$ mN/m < 0 . Therefore, the oil would not cloak the droplet surface. Based on this prediction and evaporation behavior, cloaking of droplets does not seem to occur. In addition, the wetting ridge of lubricant oil around the droplet is negligibly small.

EWOD + SLIPS: contact angle change and droplet transportation

The EWOD devices integrated with the SLIPS are tested for contact angle change and droplet transportation. First, the contact angle change is measured as the applied voltage changes, as shown in Fig. 4a. Before saturation, in general, the behavior follows the linear relation of the cosine difference of contact angle to the voltage square that is described by the Lippmann-Young equation. The required voltage becomes higher than that without the SLIPS since the SLIPS contributes to an additional dielectric layer as well.

The function of EWOD can be destructed by biofouling when highly concentrated proteins are in the working droplet. Fig. 4b shows the contact angle after EWOD is turned on at a certain voltage for 1 second and then off (Supplementary Video 3). The horizontal axis in Fig. 4b denotes the voltage when EWOD is turned on. The contact angle on the Teflon surface does not return to the initial contact angle, but is decreased as EWOD experiences higher voltages. However, the contact angle on the SLIPS returns to the initial value no matter how high voltage has been applied in the range of over 200 V. The anti-biofouling property⁴⁴ of the SLIPS is retained even with highly concentrated proteins, which critically benefits practical digital microfluidics.

In Fig. 5, a variety of conductive as well as dielectric droplets are transported by sequentially powering the electrodes from right to left (Supplementary Videos 4 and 5). Figures 5a and 5b show DI water and 1 mg/mL protein droplets transporting at 350 V, respectively. Figures 5c and 5d show the transporting of highly conductive fluids, saline at 350 V and ionic liquid at 275 V, respectively. All the working frequencies are 1 kHz in this article. Figs. 5e-h show that the droplets of complex fluids are transported on the SLIPS. It was observed that without the SLIPS the molecules and other substances in the droplets were quickly and easily adsorbed to the hydrophobic Teflon surface, making the droplets extremely difficult to move by EWOD. As shown in Fig. 4e, the sheep blood can be also transported on the SLIPS at 300 V with speed of 0.25 mm/s. The contact angle hysteresis and the tilting angle of blood (1.5 μ L) on SLIPS are 15.0° and 21°, respectively. Figs. 5f and 5g show the transporting of whole milk (on the SLIPS the contact angle hysteresis 11.3°, and the tilting angle of 1.5 μ L is 18°) and DNA solution at 350 V, with speed of 0.5 mm/s and 1.5 mm/s, respectively. The present

device is effective even for sticky fluid (e.g., honey with speed of 0.06 mm/s, Fig. 5h) because the adhesion force on the SLIPS is small enough to be overwhelmed by EWOD. The viscosity of honey is approximately 10,000 times larger than water, and it is prone to adhere to solid surfaces, rendering it challenging to operate by conventional EWOD microfluidics. It is worthwhile to mention that the antifouling property of the device remains similar after 3 months, showing a long-term stability.

The split hexagonal electrodes can transport dielectric fluids on the SLIPS as well, as shown in Figs. 5i, j and k (Supplementary Video 6): light crude oil at 250 V, propylene carbonate at 200 V, and isopropyl alcohol (IPA) at 200 V, respectively. Although the shape of electrodes used is the same as that of EWOD, the driving mechanism is liquid dielectrophoresis (L-DEP)^{61,62}, not EWOD. In L-DEP, the gap between the electrodes generates strong non-uniform electric fields^{63,64} that stretch the droplet along the electrode gap line, while EWOD decreases the contact angle over the wide region of the advancing front in the droplet and thus enhances wetting (Supplementary Fig. 2).

Lifetime characterization: cyclic EWOD actuations

In addition to the hydrophobic interactions, the prolonged operation of EWOD may accelerate biofouling, rendering it more challenging to transport droplets in digital microfluidics. Therefore, cyclic EWOD operations are evaluated for repeatability and reversibility, which are critical for real applications. The contact angle behavior in the configuration of sessile droplet is first examined under cyclic EWOD actuations (Figs. 6a-d, Supplementary Video 7). On the Teflon surface, the span of contact angle change of the protein droplet is gradually decreasing as the cycles increase, showing the deteriorating of EWOD. On the SLIPS, however, the span of the contact angle change remains almost constant, showing good reversibility and a long lifetime.

Another method to evaluate reversibility and repeatability is to laterally reciprocate a protein droplet left and right. The numbers of successful reciprocating cycles are shown in Fig. 6e. For a low concentrated (0.02 mg/mL) protein on the Teflon surface, the number of successful operation cycles is 44. For the moderate (1 mg/mL) and high (50 mg/mL) concentrations of the protein, the droplets on the Teflon surface are not able to be moved even one step because of substantial biofouling. However, on the SLIPS, over 300 successful cycles are achieved for each concentration. Even over 300 cycles, the device still maintains high performance. Detailed comparisons are shown in Supplementary Videos 8 and 9. The depletion of the lubricant was taken into account in many applications^{45,65}. In our experiment, the relocation of lubricant during transporting is mainly caused by the EWOD force. A small amount of lubricant dissipates along the contact line during the cyclic motions. However, due to the wicking property of SLIPS, the oil will replenish to that area with time. Moderate voltage and low motion frequency help the recovery of lubricant oil to the contacting area.

Recapturing dried proteins

To the authors' perspective, robust anti-biofouling means that the adhesion of bio-molecules to device surfaces is not only negligibly small but adhered bio-molecules should also be easily removed without much effort. To further evaluate the robustness of SLIPS, re-capturing dried proteins is examined. As shown in Figs. 7 (Supplementary Video 10), after drying the protein droplets, a fresh DI water droplet is transported over the dried protein spot to dissolve the protein and then wash it away while the water droplet is moving away. On the Teflon surface, an EWOD-actuated fresh water droplet can dissolve the dried proteins on the surface well but cannot wash them away (the droplet cannot completely depart from the second right electrode as shown in the fourth photo of Fig. 7a). The droplet is still pinned to the electrodes over which the proteins dried, because the proteins adsorb on the surface. The strong adhesion force interacting with adsorbed proteins is not overcome by EWOD. Such surface is contaminated and damaged permanently for EWOD actuation. Even after manually removing the proteins by using a fresh water droplet such that any dried proteins have not been clearly observed by naked eyes, EWOD could not actuate a fresh water droplet on the dried spot to move, which is pinned at the contaminated area (Supplementary Video 11).

In contrast, on the SLIPS, the dried proteins (formed a tiny dot) can be dissolved and washed away easily by an EWOD-actuated fresh water droplet without leaving any noticeable proteins on the SLIPS (inset in Fig. 7b). This process can be applied to sampling and self-cleaning.

Conclusions

This article presents antibiofouling performance when a slippery lubricant infused surface (SLIPS) is integrated with electrowetting-on-dielectric (EWOD). Instead of the solid hydrophobic layer used in the conventional EWOD-based digital microfluidics, a lubricant infused porous film is attached to the surface. The thin lubricant oil layer minimizes direct contact between the solid surface and bio-solutions, even under high electric potential. As a result, it confers the device with low contact angle hysteresis and excellent anti-biofouling performance in a wide range of protein concentrations (up to 50 mg/mL BSA), making it realizable to transport a variety of liquid solutions (conductive as well as dielectric liquids including DI water, saline solution, ionic liquid, DNA solution, whole milk, sheep blood, honey, crude oil, propylene carbonate, and isopropyl alcohol) by EWOD or L-DEP. In addition, the present EWOD integrated with SLIPS demonstrates high robustness and long lifetime in anti-biofouling performance, evidenced by long cyclic operations and successful recapturing of dried proteins. Eventually, the present EWOD configuration with SLIPS may serve as a general platform to drive a wide range of conductive and dielectric fluids (even high viscosity fluids), extending digital microfluidics to more practical applications.

Conflicts of interest

There are no conflicts to declare.

Acknowledgements

This work was in part supported by the DARPA subcontract through BAE Systems.

Notes and references

- 1 L. Qi, Y. Niu, C. Ruck and Y. Zhao, *Lab Chip*, 2019, **19**, 223-232.
- 2 M. J. Jebrail, A. H. C. Ng, V. Rai, R. Hili, A. K. Yudin and A. R. Wheeler, *Angew. Chem. Int. Edit.*, 2010, **49**, 8625-8629.
- 3 M. J. Jebrail and A. R. Wheeler, *Anal. Chem.*, 2009, **81**, 330-335.
- 4 A. E. Kirby and A. R. Wheeler, *Anal. Chem.*, 2013, **85**, 6178-6184.
- 5 V. N. Luk and A. R. Wheeler, *Anal. Chem.*, 2009, **81**, 4524-4530.
- 6 L. Malic, D. Brassard, T. Veres and M. Tabrizian, *Lab Chip*, 2010, **10**, 418-431.
- 7 E. M. Miller and A. R. Wheeler, *Anal. Chem.*, 2008, **80**, 1614-1619.
- 8 H. H. Shen, S. K. Fan, C. J. Kim and D. J. Yao, *Microfluid. Nanofluid.*, 2014, **16**, 965-987.
- 9 A. R. Wheeler, *Science*, 2008, **322**, 539-540.
- 10 V. Srinivasan, V. K. Pamula and R. B. Fair, *Lab Chip*, 2004, **4**, 310-315.
- 11 M. J. Jebrail, M. S. Bartsch and K. D. Patel, *Lab Chip*, 2012, **12**, 2452-2463.
- 12 S. K. Cho, H. Moon and C.-J. Kim, *J. Microelectromech. Syst.*, 2003, **12**, 70-80.
- 13 M. G. Pollack, A. D. Shenderov and R. B. Fair, *Lab Chip*, 2002, **2**, 96-101.
- 14 H. Geng, J. Feng, L. M. Stabryla and S. K. Cho, *Lab Chip*, 2017, **17**, 1060-1068.
- 15 A. H. Ng, M. D. Chamberlain, H. Situ, V. Lee and A. R. Wheeler, *Nature Commun.*, 2015, **6**, 7513.
- 16 J. L. Garcia-Cordero and Z. H. Fan, *Lab Chip*, 2017, **17**, 2150-2166.
- 17 S. K. Yang, X. M. Dai, B. B. Stogin and T. S. Wong, *P. Natl. Acad. Sci. USA*, 2016, **113**, 268-273.
- 18 E. Samiei, M. Tabrizian and M. Hoorfar, *Lab Chip*, 2016, **16**, 2376-2396.
- 19 S. L. Freire and A. R. Wheeler, *Lab Chip*, 2006, **6**, 1415-1423.
- 20 P. C. Gach, K. Iwai, P. W. Kim, N. J. Hillson and A. K. Singh, *Lab Chip*, 2017, **17**, 3388-3400.
- 21 F. Lapierre, M. Jonsson-Niedziolka, Y. Coffinier, R. Boukherroub and V. Thomy, *Microfluid. Nanofluid.*, 2013, **15**, 327-336.
- 22 M. Rabe, D. Verdes and S. Seeger, *Adv. Colloid Interface Sci.*, 2011, **162**, 87-106.
- 23 G. Raffaini and F. Ganazzoli, *Langmuir*, 2010, **26**, 5679-5689.
- 24 W. Norde, *Colloids Surf. B*, 2008, **61**, 1-9.
- 25 M. Abdelgawad and A. R. Wheeler, *Adv. Mater.*, 2009, **21**, 920-925.
- 26 S. H. Au, P. Kumar and A. R. Wheeler, *Langmuir*, 2011, **27**, 8586-8594.

- 27 V. N. Luk, G. C. Mo and A. R. Wheeler, *Langmuir*, 2008, **24**, 6382-6389.
- 28 S.-K. Fan, Y.-W. Hsu and C.-H. Chen, *Lab Chip*, 2011, **11**, 2500-2508.
- 29 D. Brassard, L. Malic, F. Normandin, M. Tabrizian and T. Veres, *Lab Chip*, 2008, **8**, 1342-1349.
- 30 J.-Y. Yoon and R. L. Garrell, *Anal. Chem.*, 2003, **75**, 5097-5102.
- 31 M. K. Sarvothaman, K. S. Kim, B. Seale, P. M. Brodersen, G. C. Walker and A. R. Wheeler, *Adv. Funct. Mater.*, 2015, **25**, 506-515.
- 32 I. Swyer, S. von der Ecken, B. Wu, A. Jenne, R. Soong, F. Vincent, D. Schmidig, T. Frei, F. Busse and H. J. Stronks, *Lab Chip*, 2019, **19**, 641-653.
- 33 X. Hou, Y. H. Hu, A. Grinthal, M. Khan and J. Aizenberg, *Nature*, 2015, **519**, 70-73.
- 34 D. C. Leslie, A. Waterhouse, J. B. Berthet, T. M. Valentin, A. L. Watters, A. Jain, P. Kim, B. D. Hatton, A. Nedder, K. Donovan, E. H. Super, C. Howell, C. P. Johnson, T. L. Vu, D. E. Bolgen, S. Rifai, A. R. Hansen, M. Aizenberg, M. Super, J. Aizenberg and D. E. Ingber, *Nat. Biotechnol.*, 2014, **32**, 1134-1140.
- 35 H. Geng and S. K. Cho, *IEEE MEMS*. 2018. 261-264
- 36 C. Q. Wei, G. F. Zhang, Q. H. Zhang, X. L. Zhan and F. Q. Chen, *ACS Appl. Mater. Interfaces*, 2016, **8**, 34810-34819.
- 37 P. Wang, D. Zhang and Z. Lu, *Colloids and Surfaces B: Biointerfaces*, 2015, **136**, 240-247.
- 38 N. MacCallum, C. Howell, P. Kim, D. Sun, R. Friedlander, J. Ranisau, O. Ahanotu, J. J. Lin, A. Vena, B. Hatton, T. S. Wong and J. Aizenberg, *ACS Biomater. Sci. Eng.*, 2015, **1**, 43-51.
- 39 A. K. Epstein, T. S. Wong, R. A. Belisle, E. M. Boggs and J. Aizenberg, *P. Natl. Acad. Sci. USA*, 2012, **109**, 13182-13187.
- 40 T. S. Wong, S. H. Kang, S. K. Y. Tang, E. J. Smythe, B. D. Hatton, A. Grinthal and J. Aizenberg, *Nature*, 2011, **477**, 443-447.
- 41 Q. Wei, C. Schlaich, S. Prevost, A. Schulz, C. Bottcher, M. Gradzielski, Z. H. Qi, R. Haag and C. A. Schalley, *Adv. Mater.*, 2014, **26**, 7358-7364.
- 42 H. L. Liu, P. C. Zhang, M. J. Liu, S. T. Wang and L. Jiang, *Adv. Mater.*, 2013, **25**, 4477-4481.
- 43 J. Cui, D. Daniel, A. Grinthal, K. Lin and J. Aizenberg, *Nat. Mater.*, 2015, **14**, 790-795.
- 44 A. K. Epstein, T.-S. Wong, R. A. Belisle, E. M. Boggs and J. Aizenberg, *Proc. Natl. Acad. Sci.*, 2012, **109**, 13182-13187.
- 45 A. Grinthal and J. Aizenberg, *Chem. Mater.*, 2013, **26**, 698-708.
- 46 P. Kim, M. J. Kreder, J. Alvarenga and J. Aizenberg, *Nano Lett*, 2013, **13**, 1793-1799.
- 47 K. C. Park, P. Kim, A. Grinthal, N. He, D. Fox, J. C. Weaver and J. Aizenberg, *Nature*, 2016, **531**, 78-82.
- 48 A. N. Banerjee, S. Z. Qian and S. W. Joo, *J. Colloid. Interf. Sci.*, 2011, **362**, 567-574.
- 49 D. Daniel, J. V. I. Timonen, R. P. Li, S. J. Velling and J. Aizenberg, *Nat Phys*, 2017, **13**, 1020-1025.
- 50 Y. Huang, B. B. Stogin, N. Sun, J. Wang, S. K. Yang and T. S. Wong, *Adv. Mater.*, 2017, **29**, 1604641.
- 51 X. M. Dai, B. B. Stogin, S. K. Yang and T. S. Wong, *Acs Nano*, 2015, **9**, 9260-9267.
- 52 C. Hao, Y. Liu, X. Chen, Y. He, Q. Li, K. Li and Z. Wang, *Sci. Rep.*, 2014, **4**, 6846-6852.
- 53 W. W. Cui, M. L. Zhang, D. H. Zhang, W. Pang and H. Zhang, *Appl. Phys. Lett.*, 2014, **105**, 013509.
- Z. Brabcova, G. McHale, G. G. Wells, C. V. Brown and M. I. Newton, *Appl. Phys. Lett.*, 2017, **110**, 121603.
- X. He, W. Qiang, C. Du, Q. Shao, X. Zhang and Y. Deng, *J Mater. Chem. A*, 2017, **5**, 19159-19167.
- U. C. Yi and C. J. Kim, *J. Micromech. Microeng.*, 2006, **16**, 2053-2059.
- X. Yao, Y. Hu, A. Grinthal, T. S. Wong, L. Mahadevan and J. Aizenberg, *Nat Mater*, 2013, **12**, 529-534.
- C. Semperebon, G. McHale and H. Kusumaatmaja, *Soft Matter*, 2017, **13**, 101-110.
- G. McHale, B. V. Orme, G. G. Wells and R. Ledesma-Aguilar, *Langmuir*, 2019, **35**, 4197-4204.
- J. H. Guan, G. G. Wells, B. Xu, G. McHale, D. Wood, J. Martin and S. Stuart-Cole, *Langmuir*, 2015, **31**, 11781-11789.
- T. B. Jones, *J. Electrostatics*, 2001, **51**, 290-299.
- T. B. Jones, *Langmuir*, 2002, **18**, 4437-4443.
- G. McHale, C. V. Brown, M. I. Newton, G. G. Wells and N. Sampara, *Phys. Rev. Lett.*, 2011, **107**, 186101-186104.
- Z. Brabcova, G. McHale and G. G. Wells, *Langmuir*, 2016, **32**, 10844-10850.
- P. Wang, D. Zhang, S. M. Sun, T. P. Li and Y. Sun, *ACS Appl. Mater. Interfaces*, 2017, **9**, 972-982.

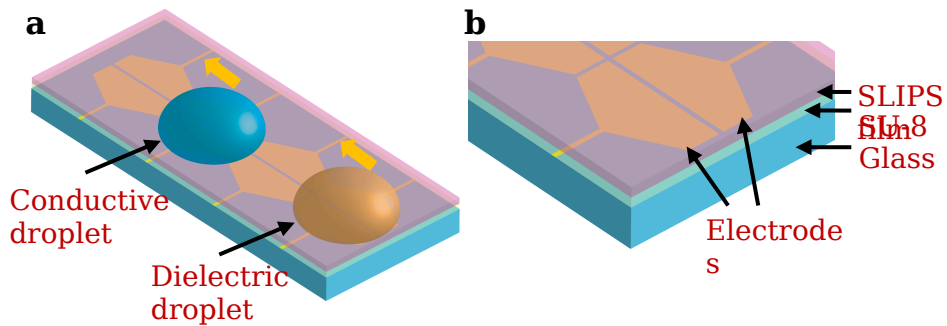


Fig. 1 Schematic of experimental device. **a**, an array of hexagonal electrodes is fabricated on the glass substrate, as the transporting pathway of the droplets. Note that each hexagonal electrode is split into two sections with a gap in the middle to drive droplets in the co-planar electrode configuration. The blue droplet denotes the conductive droplet, while the brown one represents the dielectric droplet. The yellow arrows show the moving directions of the droplets, when powering on the electrodes underneath each droplet. **b**, Zoomed view of the device to show the layer configuration.

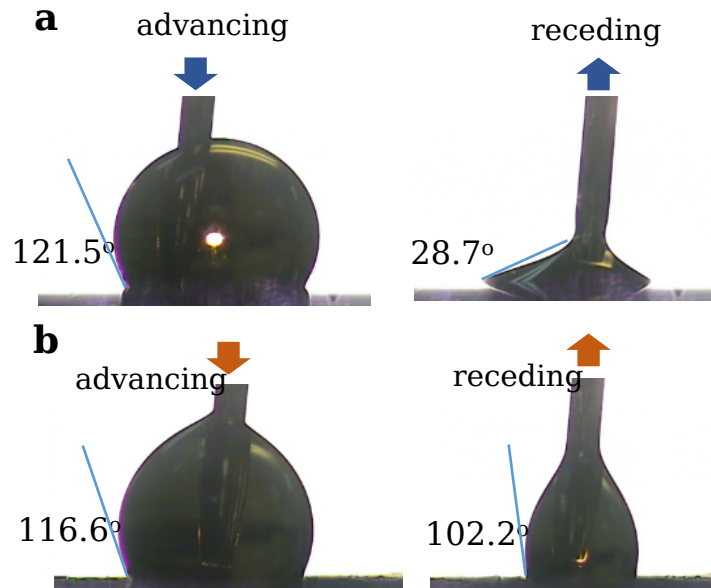


Fig. 2. Advancing and receding contact angles on Teflon surface and SLIPS. a, When adding 1 mg/mL protein on Teflon, the advancing contact angle is $121.5^\circ \pm 1.7^\circ$. When removing it, the receding contact angle is $28.7^\circ \pm 2.9^\circ$. The contact angle hysteresis on Teflon is 92.8° . b, The advancing contact angle on SLIPS is $116.6^\circ \pm 1.5^\circ$ and the receding contact angle is $102.2^\circ \pm 3.5^\circ$. The contact angle hysteresis is 14.4° . The uncertainties (standard deviation) were obtained from 5 experiments for each case.

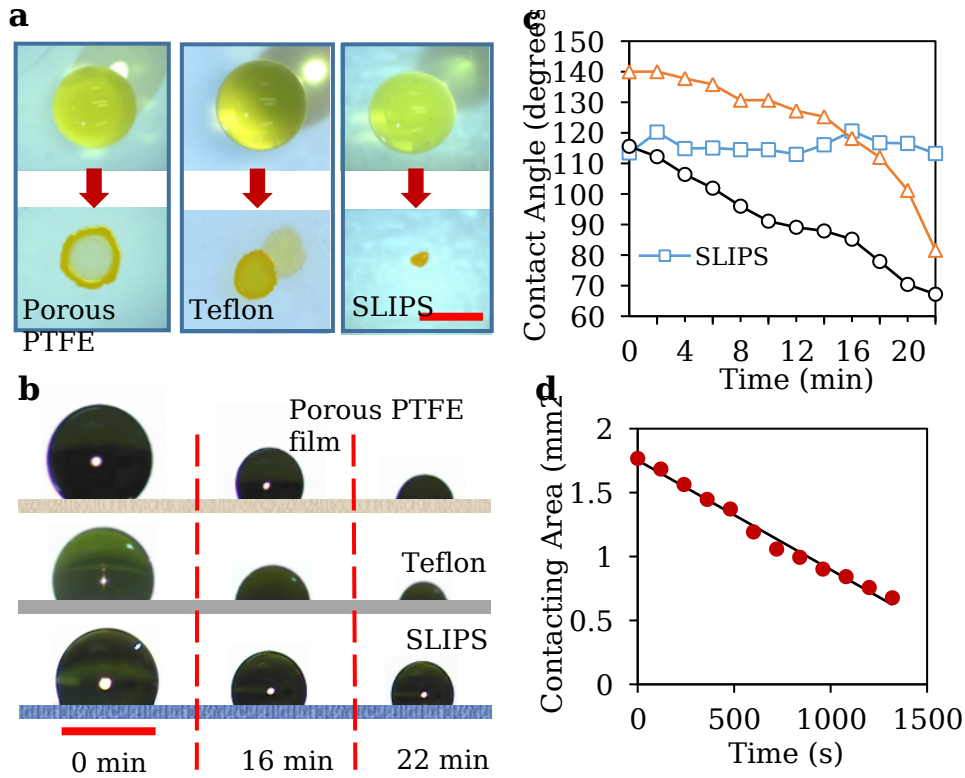


Fig.3 Evaporation of protein droplets on three different surfaces at room temperature. The protein droplets are 1.5 μL in volume with concentration of 1 mg/mL. **a**, Top views of evaporation process on three different surfaces (see Supplementary Video 1). **b**, Side views of evaporating droplets at 0 min, 16 min and 22 min. **c**, Contact angles of protein droplets on three different surfaces during evaporation. **d**, Contacting area of droplet on SLIPS vs time during evaporation. The solid line is a linear curve fitting. Scale bars: 1.5 mm.

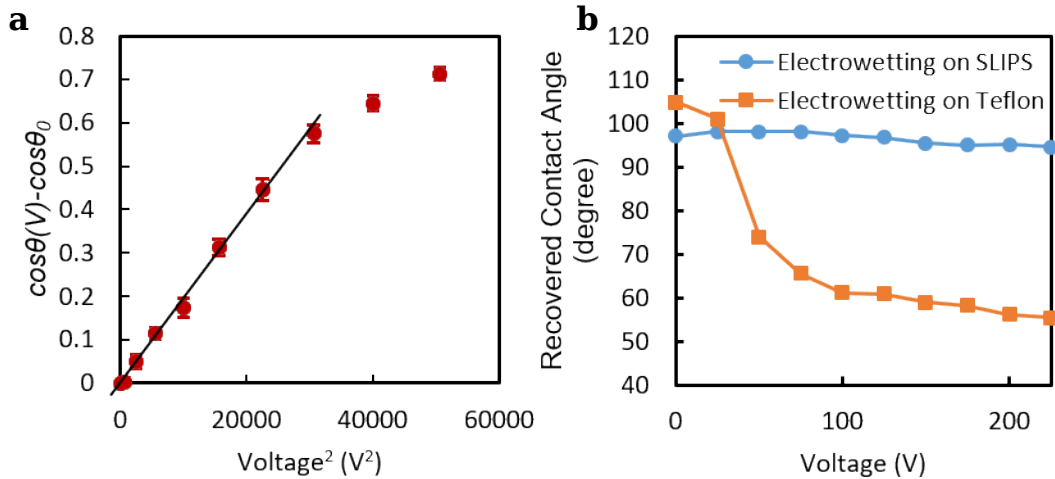


Fig. 4 EWOD-driven contact angle with 50 mg/mL protein droplet. a, Contact angle versus applied voltage on SLIPS. The behavior is similar to the Lippman-Young relation. The solid line is a linear curve fitting. The uncertainties (standard deviation) were obtained from 5 experiments. b, After applying a voltage to the droplet and then turning it off, the recovered contact angle is measured to evaluate reversibility (see Supplementary Video 3). On SLIPS, in the entire range of the voltage applied (0 V ~ 225 V), the contact angles are almost fully recovered to the initial contact angle. However, on the Teflon surface, the contact angles are not able to return to the initial state but remain at the minimum angle the droplet experiences while the voltage is turned on. As the voltage increases, the recovered contact angle is small and flattened.

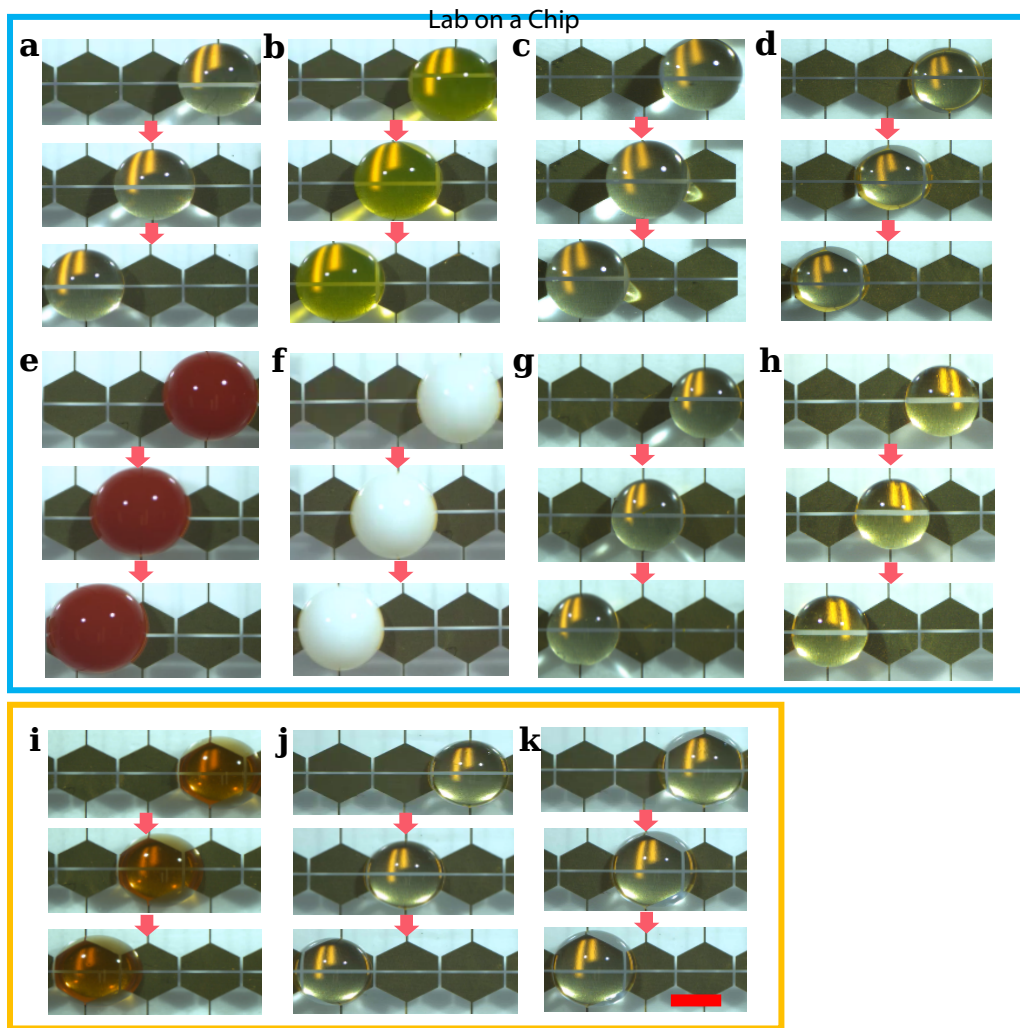


Fig. 5 Snapshots of transporting of conductive (**a - h**) and dielectric (**i - k**) droplets on the SLIPS (see Supplementary Videos 4, 5 and 6). The droplets are transported by sequentially turning the middle and left electrode electrodes on. **a**, DI water, 350 V. **b**, 1 mg/mL protein solution, 350 V. **c**, Saline, 350 V. **d**, Ionic liquid, 275 V. **e**, Sheep blood, 300 V. **f**, Whole milk, 350 V. **g**, DNA solution, 350 V. **h**, Honey, 450 V. **i**, Light crude oil, 250 V. **j**, Propylene carbonate, 200 V. **k**, IPA, 200 V. All signal frequencies are at 1 kHz. Scale bar: 1.5 mm.

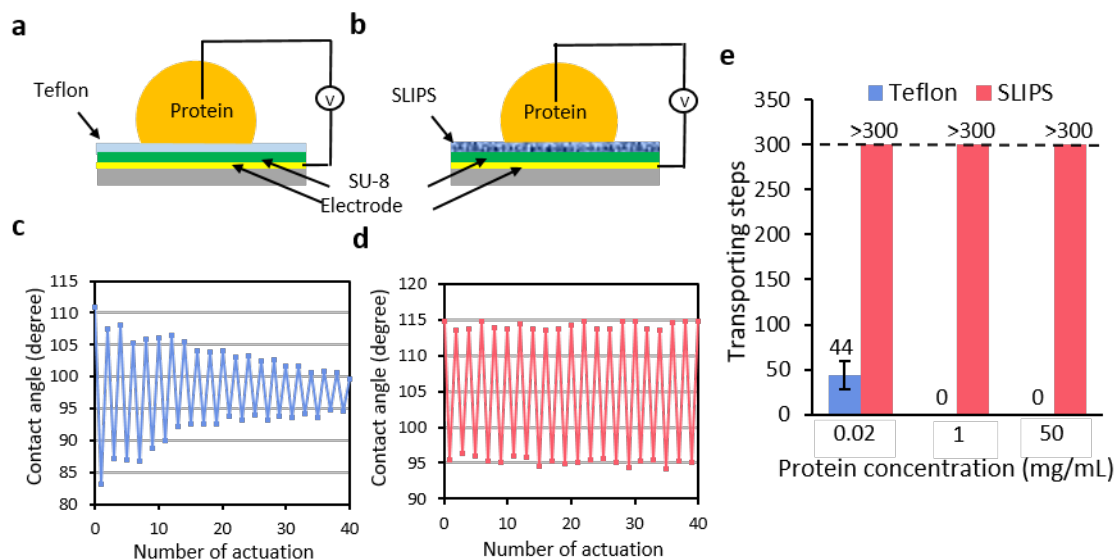


Fig. 6 Cyclic EWOD operation of sessile protein (1 mg/mL) droplet on SLIPS: anti-biofouling performance of SLIPS in EWOD digital microfluidics. a, On Teflon surface. b, On SLIPS. c, Contact angle on Teflon surface. The EWOD actuations are repeated with 75 V applied for 1 s, and then 0 V for 2 s. d, Contact angle on SLIPS; the actuations are repeated at 175 V and 0 V with the same duty cycle as Fig. 6c (see Supplementary Video 7 for c and d). e, Protein droplets (1 mg/mL) on the Teflon surface and SLIPS are cyclically transported left and right (see Supplementary Video 8), and then the number of successful cyclic operations is counted, respectively. On SLIPS, the experiment stops at 300 cycles, although more cyclic operations are possible. Each experiment was carried out five times and averaged, and the error bar represents standard deviation. The uncertainties (standard deviation) were obtained from 5 experiments.

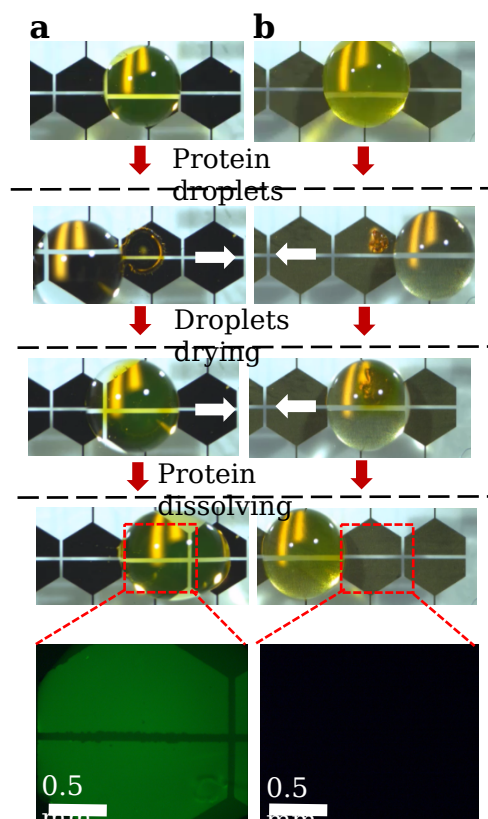


Fig. 7 Sequential snapshots of re-capturing dried proteins by a fresh DI water droplet after evaporating protein droplets on Teflon surface **a**) and SLIPS **b**), respectively (see Supplementary Video 10). **a**), on Teflon surface, a fresh DI water droplet can dissolve dried proteins. The droplet is stretched, but cannot be moved to the right completely (150 V) because of the biofouled proteins. The inset shows the fluorescent proteins biofouled on the second right electrode surface **b**), On SLIPS, the fresh DI water droplet can dissolve the dried protein completely and can be transported to the left smoothly (300 V). The inset shows no fluorescent proteins remained on the second right electrode surface.